ACS OMEGA

http://pubs.acs.org/journal/acsodf

Article

Low−Medium Temperature-Selective Catalytic Reduction of NO with NH_3 over a Mn/Co-MOF-74 Catalyst

Zhonghao Sun, Xue Mi, Yichen Luo, Siyuan Wang, Bo Yuan, Runlong Hao, and Yi Zhao*

Cite This: *ACS Omega* 2021, 6, 34347−34358

Read Online

ACCESS | Metrics & More | Article Recommendations

ABSTRACT: To realize the selective catalytic reduction of NO at low−medium temperatures and avoid secondary pollution, a highly active catalyst Mn/Co-MOF-74 was synthesized. X-ray diffraction, X-ray photoelectron spectroscopy, thermogravimetric analysis, Brunauer−Emmett−Teller method, and scanning electron microscopy were employed to analyze the physicochemical properties of catalysts with different Mn/Co molar ratios and conjecture about the difference in the catalytic activity. Meanwhile, the effects of the molar ratio of Mn/Co, catalyst dosage, catalyst synthesis conditions, GHSV, and temperature on the NO conversion efficiencies were investigated and found that an optimal NO conversion efficiency of 93.5% was obtained at 200−225 °C. In the end, the stability of Mn/Co-MOF-74 was investigated and found that the catalyst has better sulfur and water resistance, and the NO conversion mechanism was speculated on the basis of characterizations and literature data.

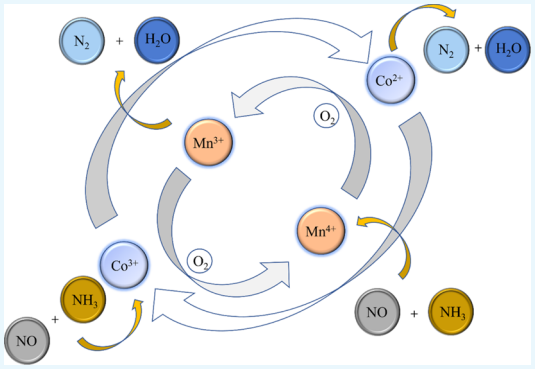

1. INTRODUCTION

As one of the main pollutants released by the burning of fossil fuels, nitrogen oxide (NO) is the main target of flue gas treatment in coal-fired power plants. If its emissions cannot be effectively controlled, it will exacerbate a series of air pollution problems such as acid rain and photochemical smog,[1−5] thereby threatening the ecosystem and human health. By now, NH_3-selective catalytic reduction (NH_3-SCR) is not only the most widely used NO_X control technology in coal-fired power plants but also in other industries such as glass, steel, cement, and so forth.[6−10] However, this technology has exposed many troubles in practical applications: the wear, blockage, poisoning, and deactivation of the catalyst occur frequently because the catalyst is usually placed in high sulfur and dusty areas to maintain the reaction temperature; meanwhile, when the power plant is at a low load, the lower flue gas temperature (200−250 °C) can hardly meet the temperature required by SCR, unless an external heat source is introduced.[11−13] Hence, it is of practical significance and commercial value to develop medium- and low-temperature SCR catalysts, which can not only arrange the SCR catalyst backward to reduce the hazards of dust and sulfur dioxide but also expand the reaction temperature and application range of NH_3-SCR.

Liu et al.[14] synthesized mesoporous $Ce_{0.8}W_{0.2}O_x$ by the mechanochemical self-assembly strategy, and a removal efficiency of 100% and a N_2 selectivity of 97% in a wide temperature range of 225−400 °C were achieved, better than those of $Ce_{0.8}W_{0.2}O_x$ prepared by the sol−gel method. Meanwhile, mesoporous $Ce_{0.8}W_{0.2}O_x$ also has excellent sulfur and water resistances. Although the removal efficiency is reduced by 15% after the addition of $SO_2 + H_2O$, it can quickly return to 95% after stopping the flow. In recent years, metal−organic framework (MOF) materials have been widely used in the field of environmental protection due to their large specific surface area, high porosity, controllable pore size, and modifiability.[15−19] In terms of NH_3-SCR over MOF materials, researchers had done a lot of work: Sun et al. prepared the Cu-BTC (BTC = benzene-1, 3, 5-tricarboxylate) catalyst and found that it had better selective adsorption of NO_x in multicomponent flue gas, which is essential for the occurrence of the SCR reaction;[20] Wang et al.[21] synthesized the MIL-100(Fe) (iron(III) 1,3,5-benzenetricarboxylate hydrate) catalyst by the hydrothermal method and utilized it to perform the SCR experiments at 200−300 °C, in which more than 80% removal efficiency was achieved, and the highest removal efficiency 99% was obtained at 275 °C. Further research adopted MIL-100(Fe) and CeO_2 as the carrier and active ingredient to prepare 0.08IM-CeO_2/MIL-100(Fe) catalysts, and the characterization results proved that the presence of CeO_2 successfully improved the oxygen absorption capacity of

Received: July 30, 2021
Accepted: November 25, 2021
Published: December 7, 2021

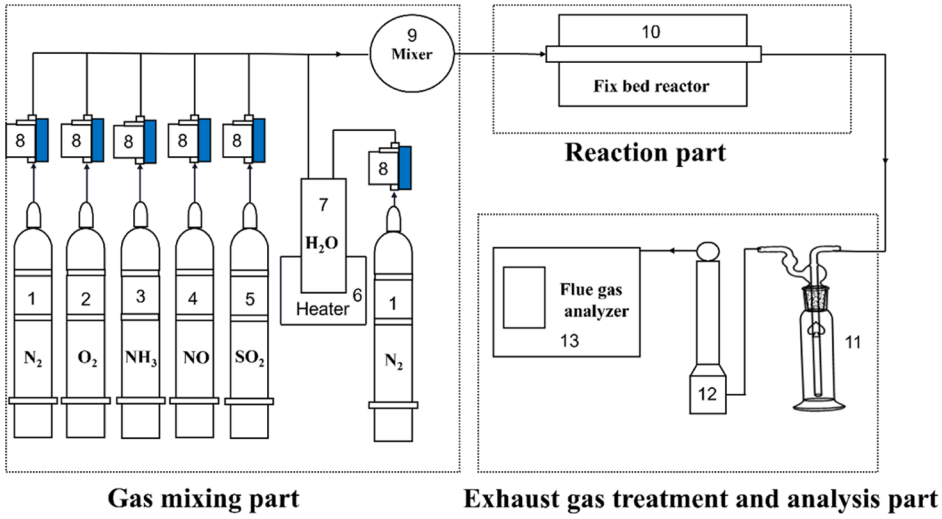

Figure 1. Schematic diagram of the experimental apparatus. (1−5) N_2, NO, SO_2, O_2, and NH_3 gas cylinders; (6) electrical heater; (7) water; (8) mass flow meters; (9) mixer; (10) fixed-bed reactor; (11) absorption bottle; (12) drying tower; and (13) multifunctional flue gas analyzer.

the composite catalyst, which is why the effective range of the catalytic temperature can be expanded to 175−300 °C. Sun et al.[22] prepared a Ni-MOF catalyst that can maintain the effective crystal structure below 440 °C using the hydrothermal synthesis method, which successfully improved the service life of the MOF catalyst. In particular, more than 90% NO_X removal efficiency was achieved in a wide temperature range of 275−400 °C. Overall, although the MOF catalyst has many advantages, its sulfur resistance and water resistance need to be improved.

According to literature, manganese-based materials are the most widely used medium- and low-temperature SCR catalysts. Kapteijn et al.[23] used manganese oxides with different valence states to conduct a series of NO_x removal experiments, and the results indicated that the valence of Mn has a great influence on the catalytic activity. Meanwhile, researchers also found that the catalytic activity of Mn-based catalysts decreases in the order of $Mn^{4+} > Mn^{3+} > Mn^{2+}$ at 177 °C. In addition, Tian et al.[24] used different methods to prepare MnO_2 in the state of nanoparticles, nanorods, and nanotubes and studied the effects of different morphologies on the denitrification efficiency and found that the removal efficiency of all catalysts at GHSV of 36 000 h^{-1} increased with the rising of the reaction temperature, among which the denitrification efficiency of nanorod MnO was the highest, reaching more than 90% at 250−300 °C and close to 100% at 300 °C. It must be pointed out that the shortcomings of the MNO_X catalyst are also obvious; the sulfur resistance of the catalyst is not strong and irreversible, and the N_2 selectivity decreases with the increase of the reaction temperature.[25] Fortunately, these defects can be overcome by doping with other elements to form binary or even ternary composite catalysts.

At present, several related studies have shown that doping Co can improve the physicochemical properties of Mn-based catalysts.[26] Boningari et al.[27] investigated the NO removal efficiency using the $MnCo/TiO_2$ catalyst and found that the addition of Co indeed improved the NO removal efficiency. Shi et al.[28] explored the sulfur resistance of Mn−Co nanorods and found that the addition of Co significantly enhanced the sulfur resistance; when 100 ppm of SO_2 was added into the reactor, the NO removal efficiency only dropped by 9%. The goal of this paper is to combine the advantages of Mn, Co, and MOF and propose a novel low−medium temperature NO removal method to avoid the above drawbacks. In detail, we will synthesize a novel Mn/Co-MOF-74 catalyst by the microwave method, and the formation and crystallization only take 4 h. Meanwhile, the influence of synthesis conditions and reaction factors on the NO removal efficiency will be investigated; the sulfur and water resistances of the catalyst and N_2 selectivity would also be evaluated. Finally, the NO removal mechanism will be speculated based on the serial characterization of reaction products and catalysts.

2. EXPERIMENTAL SECTION

2.1. Chemicals. All the chemicals were of analytical grade and purchased from Kermel Reagent Manufactories (Tianjin, China). $MnCl_2{\cdot}4H_2O$ (99%), $Co(NO_3)_2{\cdot}6H_2O$ (99%), and 2,5-dihydroxyterephthalic acid (DHTP, 99%) were used for preparing the catalyst. Deionized water, anhydrous ethanol, and methanol were used for dissolving and washing.

2.2. Synthesis of Catalysts. The MOF-74 catalyst loaded with manganese and cobalt oxides (named as Mn/Co-MOF-74) was prepared by the microwave hydrothermal method. In detail, $MnCl_2{\cdot}4H_2O$ and $Co(NO_3)_2{\cdot}6H_2O$ were mixed with DHTP (0.1333 g), DMF (53 mL), CH_3CH_2OH (8.5 mL), and H_2O (8.5 mL); then, the resulting solution was put into a Teflon-lined autoclave and heated at 130 °C in a microwave hydrothermal apparatus (XH-800S) for 4 h. After cooling to room temperature, the mother liquor was filtered out, and the products were washed and soaked in methanol for 1 h. Then, the methanol solvent was decanted and replaced every 1 h during the next 6 h, until the supernatant was transparent. The sediment was removed from the bottom and dried in an air-drying oven at 80 °C for12 h.

2.3. Characterization. Characterizations of the catalysts were performed by various methods: X-ray diffraction (XRD, Bruker D8 Advance) in the range of 10−90° with a scanning speed of 4/min was carried out to determine the composition of the catalyst. Thermogravimetric analysis (TGA, TA7000) was adopted to analyze the thermal stability of the catalyst. A scanning electron microscope equipped with a Hitachi S-4800 (Japan) system was used to observe the microstructure of the catalyst, and X-ray photoelectron spectroscopy (XPS, PHI X-tool) calibrated by the C 1s peak at 284.6 eV was conducted to

https://doi.org/10.1021/acsomega.1c04077
ACS Omega 2021, 6, 34347−34358

investigate the surface chemical composition and elemental speciation. Besides, nitrogen adsorption and desorption isotherms obtained using the Brunauer−Emmett−Teller (BET) method (Quantachrome SI) were employed to analyze the surface area of the catalyst.

2.4. Experimental Procedures. As illustrated in Figure 1, the experimental system mainly consists of simulated flue gas generation, catalytic reduction, and tail gas detection system. The core part is the catalytic reduction device, in which the selective catalytic reduction experiments of NO with NH_3 were conducted in a fixed-bed quartz reactor with approximately 0.2 g of catalyst. Before the start of the experiment, the catalysts were pretreated in nitrogen at 250 °C for 3 h, whose purpose was to remove the residual organic solvents on the surface of the catalyst. N_2, NO, NH_3, and SO_2 cylinder gases (1−4, 99.99%, North Special Gas Co., Ltd., China) controlled by mass controllers (7) were employed to simulate the flue gas, and water vapor was generated by using N_2 as the carrier gas to purge the liquid water heated by the electrical heater (6). The total flue gas flow rate of the fixed-bed quartz reactor with an inner diameter of 10 mm (10) was 300 mL/min, and the typical composition of the reactant gas was as follows: 500 ppm NO, 500 ppm NH_3, 6% O_2, 500 ppm SO_2 (only when used), and 5% H_2O (only when used). After the reaction was completed, the gas passed through the absorption bottle (11) and drying tower (12), and the concentrations of NO_x, SO_2, and O_2 were measured using a multifunctional flue gas analyzer (13) (detection limit of 1 ppm/m^3, ECOM-J2KN, German RBR company). In this paper, the NO removal efficiency (η) and N_2 selectivity were obtained from the following equation

$$\eta = \frac{NO_{in} - NO_{out}}{NO_{in}} \times 100\%$$

$$N_2\ \text{selectivity} = \frac{(NO_{in} + NH_{3in}) - (NO_{out} + NH_{3out}) - 2N_2O - NO_2}{(NO_{in} + NH_{3in}) - (NO_{out} + NH_{3out})} \times 100\%$$

3. RESULTS AND DISCUSSION

3.1. Characterization of Catalysts. In order to analyze the crystalline phase composition of the synthesized catalyst, XRD was performed, and the results are shown in Figure 2. Four characteristic peaks at 2θ = 6.7, 11.7, 24.4, and 25.7° were all observed in the spectra of the catalysts with different Mn and Co ratios, consistent with the literature data,[29−31] indicating that the synthesis of Mn/Co-MOF-74 was successful. Besides, the strength of the characteristic peak appeared to show more obvious difference with the change of the ratio of Mn and Co, proving that Mn and Co elements had been loaded successfully. It is worth noting that when the Mn/Co ratios are 3:1 and 2:1, respectively, a group of strong peaks in the range of 2θ = 18∼21° are observed, and the corresponding substances are determined as MnO_2 and Mn_2O_3 by referring to literature[32,33] because in the microwave hydrothermal synthesis process, when the Mn content is too high, the oxidation and crystallization are likely to occur on the surface of the catalyst, and the manganese component eventually exists in the stable state of MnO_2 and Mn_2O_3. Besides, when the Mn/Co ratios are 3:1 and 2:1, respectively, the characteristic peaks of Co_3O_4 also appear at 27.5 and 32.9°. Overall, it can be concluded that the molar ratio of Mn/Co is a

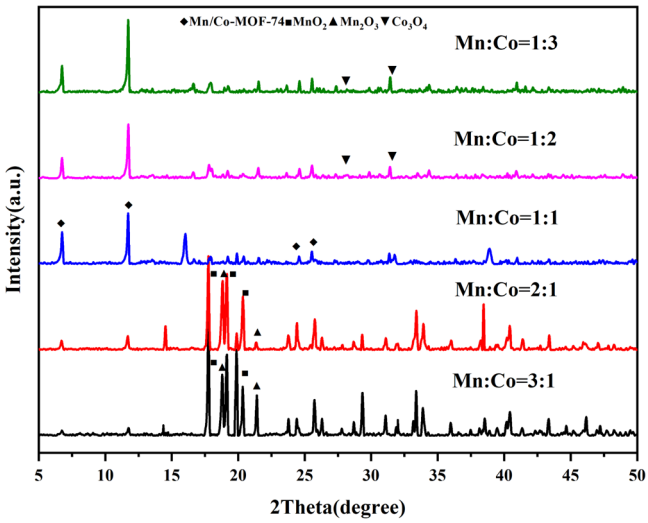

Figure 2. XRD patterns of Mn/Co-MOF-74.

key synthesis factor, and oxides will be formed on the surface of the catalyst and affect the NO removal efficiency when the content of Mn or Co is too high.

XPS was also used to explore the surface elemental composition and valence of the Mn/Co-MOF-74 catalyst. As depicted in Figure 3a, it can be found that the Co element presents four characteristic peaks within 770−815 eV, and the height of the characteristic peak changes with the content of Co in the catalyst. According to literature reports,[34,35] for Co 2p, the two main peaks at 781.7 and 797.6 eV are attributed to Co^{3+} and Co^{2+}, respectively, and the peaks at about 803.2 and 786.5 eV are attributed to the satellite peaks. This shows that the Co element exists on the surface of the catalyst in two valences: Co^{2+} and Co^{3+}. As shown in Table 1, the relative atomic percentage concentration of Co^{3+}/Co is higher than that of Co^{2+}/Co. Generally, Co^{3+} is much more reactive than Co^{2+} because of its stronger redox ability.

The Mn 2p spectra of five catalysts are presented in Figure 3b, which are mainly divided into two categories: the peak centers at 654.3 and 643.1 eV can be explained as Mn^{4+}, and the peak at 641.7 eV is assigned to Mn^{3+}.[36−41] As shown in Table 1, the percentage of Mn^{4+}/Mn on Mn/Co-MOF-74 is higher than that of Mn^{3+}/Mn. According to the reports, Mn^{4+} participates in the reversible oxidation−reduction reaction cycle, which can improve the ability of NO to oxidize to NO_2, being beneficial for promoting the rapid SCR reaction.[42] It can be seen from Figure 3c that the types of O on the catalyst surface are mainly divided into two types: the peak centers at 532.3−532.6 eV are explained as O in C−OH, and another oxygen peak at 531.7−531.9 eV is assigned to C═O.[43,44] Overall, it can be concluded that the main surface active substances of Mn/Co-MOF-74 are Co^{3+} and Mn^{4+}; abundant Mn^{4+} and Co^{3+} are presented on the surface of the Mn/Co-MOF-74 catalyst, which is considered to be one of the factors for increasing the catalytic activity.

To determine the structural change and thermal stability of the prepared Mn/Co-MOF-74 catalyst, TG experiments were performed, and the results are shown in Figure 4. The mass loss of Mn/Co-MOF-74 catalysts with different ratios is roughly similar. For the catalyst with Mn/Co = 1:1, three significant stages of mass loss were observed during the experiment:[45] in the first stage, at 30−150 °C, the catalyst mass

https://doi.org/10.1021/acsomega.1c04077
ACS Omega 2021, 6, 34347−34358

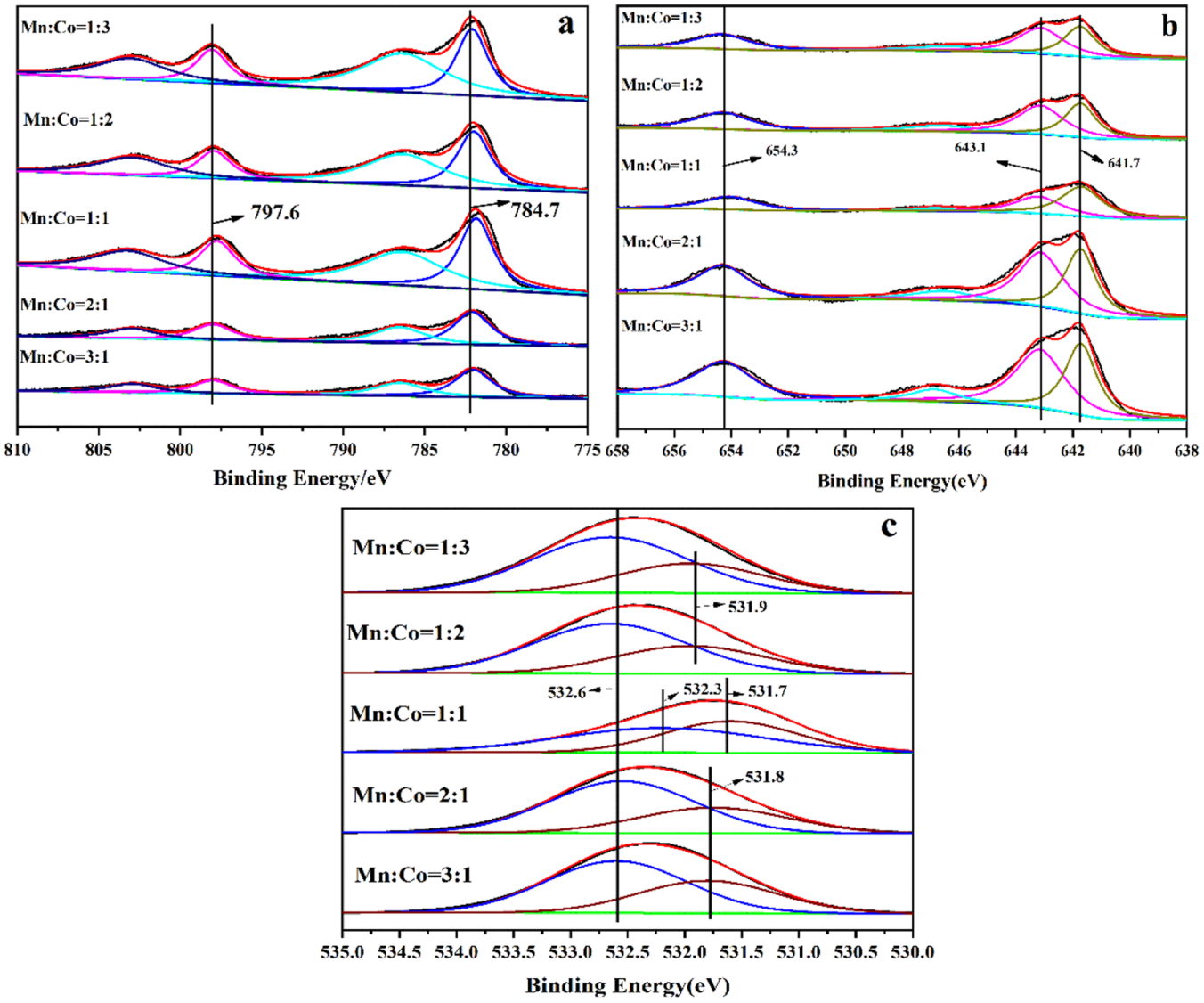

Figure 3. XPS spectra of Co (a), Mn (b), and O (c).

Table 1. Relative Atomic Percentages of Different Valence Elements

	percent of valence state % (binding energy, eV)					
catalysts	Mn^{4+}	Mn^{3+}	Co^{3+}	Co^{2+}	Mn^{4+}/Mn^{3+}	Co^{3+}/Co^{2+}
Mn/Co = 3:1	76.47	23.53	65.72	34.28	3.25	1.92
Mn/Co = 2:1	72.59	27.41	65.13	34.87	2.65	1.87
Mn/Co = 1:1	62.49	37.51	65.81	34.19	1.67	1.92
Mn/Co = 1:2	72.18	27.82	66.51	33.49	2.59	1.99
Mn/Co = 1:3	72.85	27.15	67.48	32.52	2.68	2.08

loss was 16.5%, mainly due to H_2O and methanol on the catalyst surface; in the 150−316 °C stage, the mass loss of the catalyst was about 13.1%, mainly due to the solvent DMF on the surface of the catalyst. The final stage is at 316−576 °C, in which the structure of the catalyst begins to collapse, and it is completely destroyed at 576 °C. The above results indicate that the activation of the catalyst at 200 °C before the experiment can effectively remove the residual solvent on the surface of the catalyst, exposing more active sites of the catalyst, which is beneficial to the SCR reaction.

The textural properties of Mn/Co-MOF-74 catalysts were measured at −196 °C and summarized in Table 2 It can be found that with the change of the molar ratio, the catalyst with Mn/Co = 1:1 has the largest BET surface area and pore volume and the smallest pore size, which are 212.84 m/g, 0.24 cm^3, and 3.94 nm, respectively.

Pore size distribution (Figure 5) has shown that the Mn/Co-MOF-74 catalyst is a mesoporous material, and the pore size is mainly distributed in the range 3−6 nm. The pore volume of Mn/Co = 1:1 is larger than the other ratio catalysts. Combined with the XRD results, there are some oxides like MnO_2 and Mn_2O_3 or Co_3O_4 on the surface of Mn/Co-MOF-74 catalysts with other molar ratios; this may be the reason for the reduction of the specific surface area. When Mn/Co = 1:1,

https://doi.org/10.1021/acsomega.1c04077
ACS Omega 2021, 6, 34347−34358

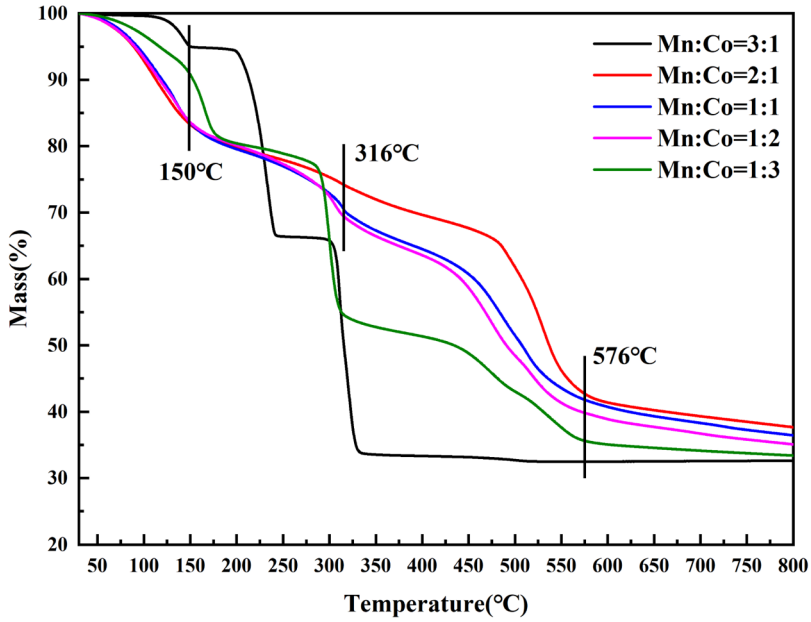

Figure 4. TG curves of the Mn/Co-MOF-74 catalyst.

Table 2. Summary of the Textural Parameters of the Catalysts

catalysts	pore volume (cm^3/g)	BET surface area (m^2/g)	pore size (nm)
Mn/Co = 3:1	0.06	35.99	6.60
Mn/Co = 2:1	0.04	59.44	6.03
Mn/Co = 1:1	0.24	212.84	3.94
Mn/Co = 1:2	0.09	72.82	5.01
Mn/Co = 1:3	0.11	103.74	4.19

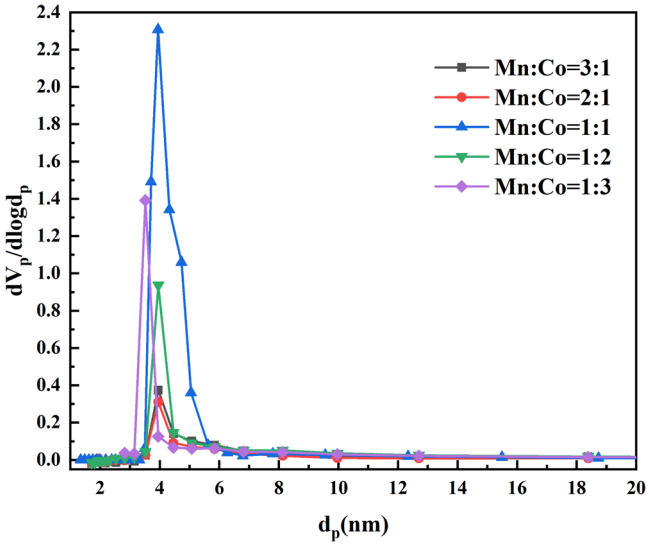

Figure 5. Pore size distribution of Mn/Co-MOF-74 catalysts.

the two metal elements exist in a coordinated form in the catalyst; the mesoporous structure of the oxide covering the catalyst is not formed on the catalyst surface, so the specific surface area of Mn/Co = 1:1 is the largest. The unique mesoporous structure with a large BET surface area helps to improve the gas adsorption capacity of the catalyst and enhance the mass-transfer rate between the active sites and NH_3 or NO, thereby improving the NO removal efficiency.

The morphology of Mn/Co-MOF-74 catalysts with different molar ratios was observed by scanning electron microscopy (SEM), and the results with different magnifications are shown in Figure 6. The catalyst with a molar ratio of Mn/Co = 3:1 has a layered lumpy morphology, and the overall particle size of the catalyst is relatively large. Combined with the XRD results, it is speculated that the generated MnO_2 and Mn_2O_3 cover the surface and make the particles bigger. When the Co content gradually increases to Mn/Co = 1:1, the particles of the catalyst change from large into small. In addition, it can be seen from Figure 5c that the surface of the catalyst has obvious edges, corners, and a regular shape, which can improve the catalytic activity. However, as the Co content further increased, the particle size of the catalyst became larger again, and some deposits appeared on the surface. XRD characterization results suggest that the deposit is Co_3O_4, which can cover the active sites on the catalyst surface, being unconducive to the catalytic reduction of NO.

3.2. Effect of Synthesis Conditions. In order to study the effect of catalyst synthesis conditions and experimental conditions on the NO removal efficiency and facilitate the subsequent industrial applications, a series of experiments were designed and carried out. It is generally believed that the synthesis conditions, especially the temperature and time, have greater impacts on the catalytic removal experiments. The effects of synthesis temperature and time on the NO removal efficiency of the Mn/Co-MOF-74 catalyst were first investigated.

It can be seen from Figure 7a that the Mn/Co-MOF-74 catalyst synthesized by the microwave method exhibits a NO removal efficiency of more than 80% at 175−250 °C. The catalyst with a synthesis temperature of 130 °C has the highest NO removal efficiency, 93.5%, at 200 °C. The effect of synthesis time on NO removal is illustrated in Figure 7b; it is not difficult to find that the catalyst synthesized in 4 h has the highest removal efficiency at each temperature, followed by 2 and 6 h. With the increasing synthesis time, the metal oxides gradually form and crystallize. Once the synthesis time is insufficient, the synthesis of oxides is incomplete; however, the

https://doi.org/10.1021/acsomega.1c04077
ACS Omega 2021, 6, 34347−34358

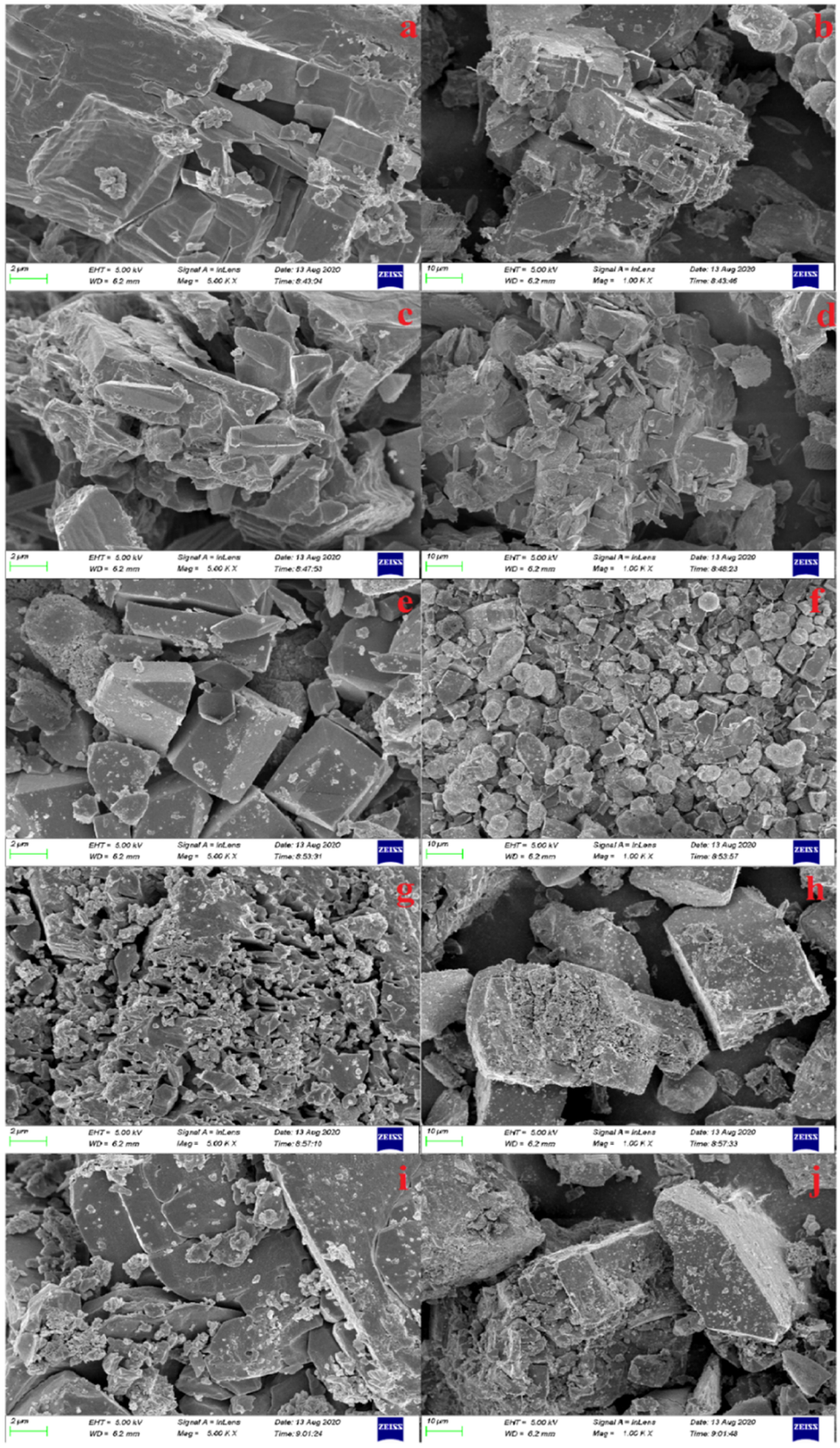

Figure 6. SEM images of Mn/Co-MOF-74 catalysts: (a,b) Mn/Co = 3:1; (c,d) Mn/Co = 2:1; (e,f) Mn/Co = 1:1; (g,h) Mn/Co = 1:2; and (i,j) Mn/Co = 1:3.

oxides will form on the surface of the catalyst if the synthesis time is too long, which would reduce the catalytic activity of the catalyst. Therefore, in this paper, the optimal synthesis time is selected as 4 h.

3.3. Effect of Molar Ratio of Mn/Co. According to the results of XRD, SEM, and BET, the catalyst with a molar ratio of Mn/Co = 1:1 has an optimal catalyst structure. To verify this result, the effect of different Mn/Co molar ratios on the

https://doi.org/10.1021/acsomega.1c04077
ACS Omega 2021, 6, 34347−34358

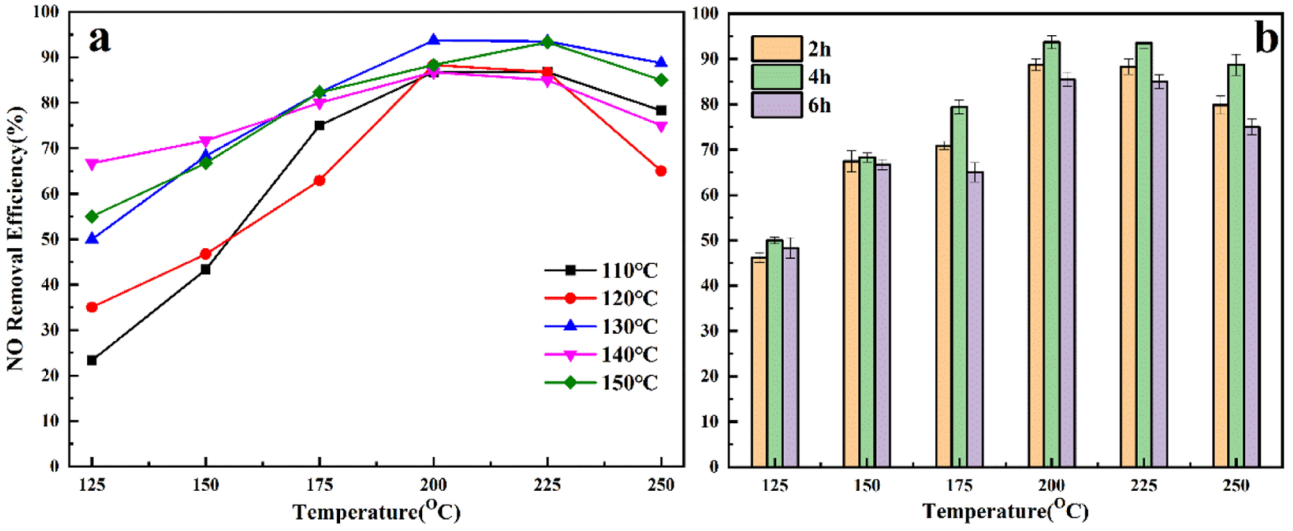

Figure 7. Effect of synthesis conditions. (a) Synthesis temperature and (b) synthesis time (flue gas flow is 600 mL/min, NO═NH_3 = 500 ppm, O_2 = 6%, and catalyst dosage = 0.2 g).

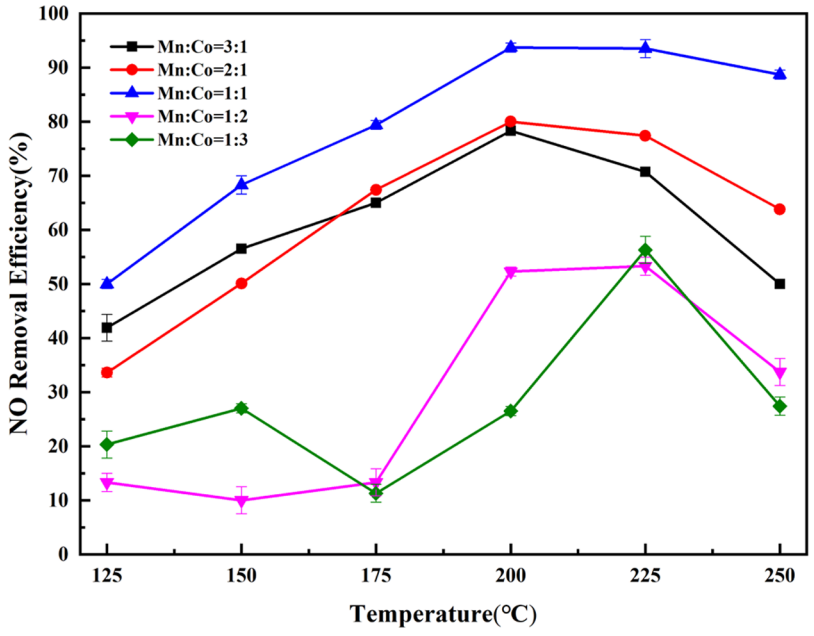

Figure 8. Effect of the molar ratio of Mn/Co (flue gas flow is 600 mL/min, NO═NH_3 = 500 ppm, O_2 = 6%, and catalyst dosage = 0.2 g).

removal efficiency of NO was performed. It can be seen from Figure 8 that when the temperature is in the range of 125−200 °C, for the catalysts with molar ratios Mn/Co = 3:1, Mn/Co = 2:1, and Mn/Co = 1:1, the NO removal efficiency increases as the temperature rises. When the temperature is between 200 and 225 °C, the NO removal efficiency reaches the highest level and then drops. In contrast, the NO removal efficiency using catalysts with molar ratios of Mn/Co = 1:2 and Mn/Co = 1:3 does not show obvious change. In particular, the highest efficiency occurred when the Mn/Co ratio was 1:1 and the reaction temperature was 200 °C, which is consistent with the analysis result of the above characterizations: the catalyst with a molar ratio of Mn/Co = 1:1 has the optimal structure and higher NO removal efficiency.

3.4. Effect of Catalyst Dosage and GHSV. It is generally considered that the catalyst dosage has a greater effect on the removal efficiency; therefore, the effect of catalyst dosage on the NO removal efficiency is investigated in this work, and the results are shown in Figure 9. It can be found that as the dosage increases from 0.1 to 0.2 g, the NO removal efficiency increases significantly from 77.6 to 93.5%. When the catalyst dosage increases from 0.2 to 0.3 g, the NO removal efficiency does not change so much. This indicates that with the increase of the catalyst dosage, the NO removal efficiency is improved, although this improvement is limited. Considering the economics of the experiment, the optimal dosage of the catalyst is chosen as 0.2 g.

The effect of GHSV on removal efficiency is also shown in Figure 9. It can be found that the removal efficiency is the highest when GHSV is 45859.9 h^{-1}. The increase of GHSV would reduce the contact time between NO/NH_3 and Mn/Co-MOF-74. When GHSV was too fast, the flue gas could not fully contact the catalyst, and the catalytic reaction was not completed, resulting in the decrease of removal efficiency.

https://doi.org/10.1021/acsomega.1c04077
ACS Omega 2021, 6, 34347−34358

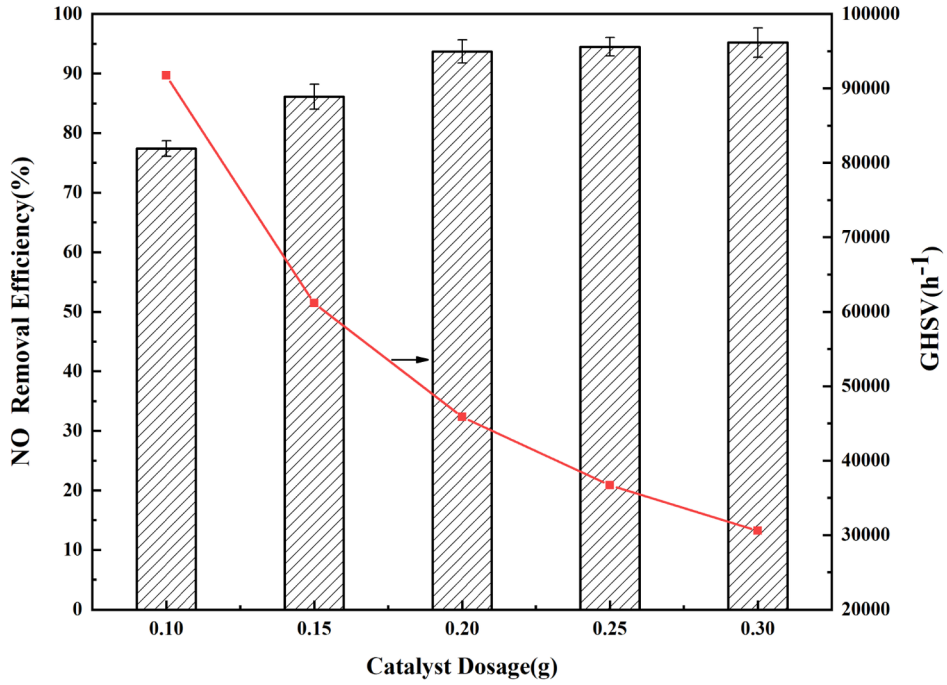

Figure 9. Effect of the catalyst dosage and GHSV (flue gas flow is 600 mL/min, NO═NH_3 = 500 ppm, O_2 = 6%, and temperature = 200 °C).

Therefore, the optimal GHSV in the experiment is 45859.9 h^{-1}.

3.5. N_2 Selectivity of Mn/Co-MOF-74. N_2O and NO_2 are the byproducts of the SCR reaction. It is meaningful to test the amount of N_2O and NO_2 produced by the Mn/Co-MOF-74 catalyst at different temperatures and calculate the N_2 selectivity. It can be seen from Figure 10 that almost no

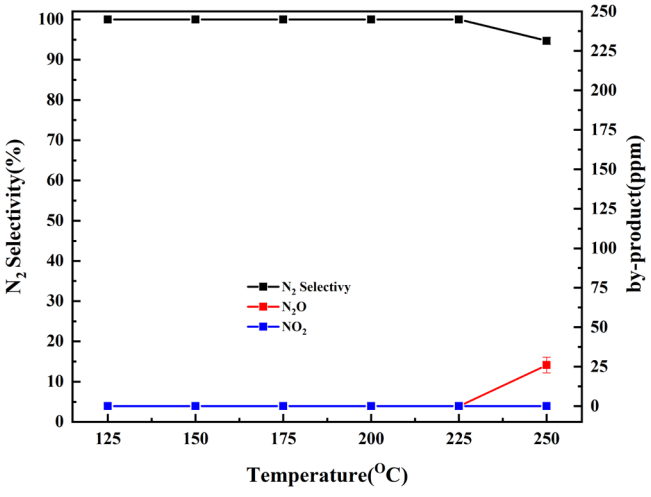

Figure 10. N_2 selectivity and N_2O generation amount (flue gas flow is 600 mL/min, NO═NH_3 = 500 ppm, O_2 = 6%, and catalyst dosage = 0.2 g).

NO_2 was generated during the entire experiment, no N_2O is generated at 125−225 °C, and a small amount of N_2O is released at 250 °C; currently, the N_2 selectivity is 94.7%. In general, the catalyst could maintain the high N_2 selectivity and NO removal efficiency.

3.6. Stability of Mn/Co-MOF-74. Stability and sulfur and water resistances are important indicators for the long-term use of low-temperature denitrification catalysts. As shown in Figure 11, the NO removal efficiency was stabilized at 90% in 16 h without SO_2 and H_2O, but when SO_2 and H_2O were added,

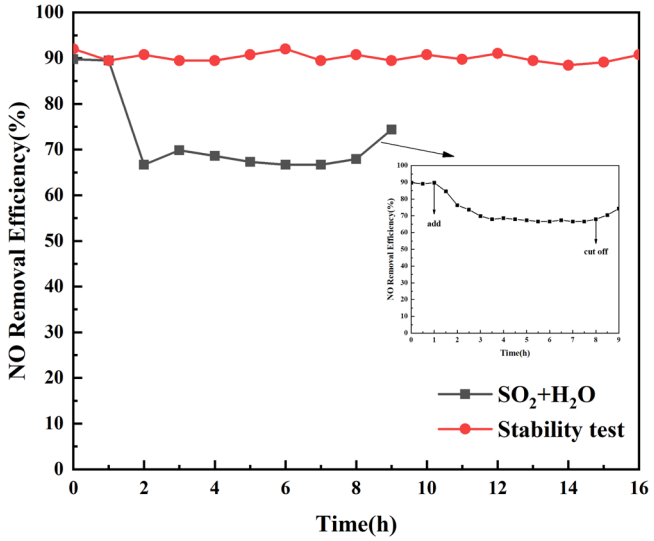

Figure 11. Stability test of Mn/Co-MOF-74 (flue gas flow is 600 mL/min, NO═NH_3 = 500 ppm, O_2 = 6%, SO_2 = 500 ppm, H_2O = 5%, catalyst dosage = 0.2 g, and temperature = 200 °C).

the NO removal efficiency dropped rapidly to 66.7% and then stabilized, partly due to the competitive adsorption of SO_2 and H_2O with the reactants, which affected the active sites on the catalyst surface. Another reason was that SO_2, H_2O, and NH_3 would generate sulfites on the surface of the catalyst, covering the catalyst active sites and decreasing the NO removal efficiency. Fortunately, after cutting off the supplements of SO_2 and H_2O, the NO removal efficiency gradually recovered to 74%, proving that the Mn/Co-MOF-74 catalyst has good sulfur and water resistances.

https://doi.org/10.1021/acsomega.1c04077
ACS Omega 2021, 6, 34347−34358

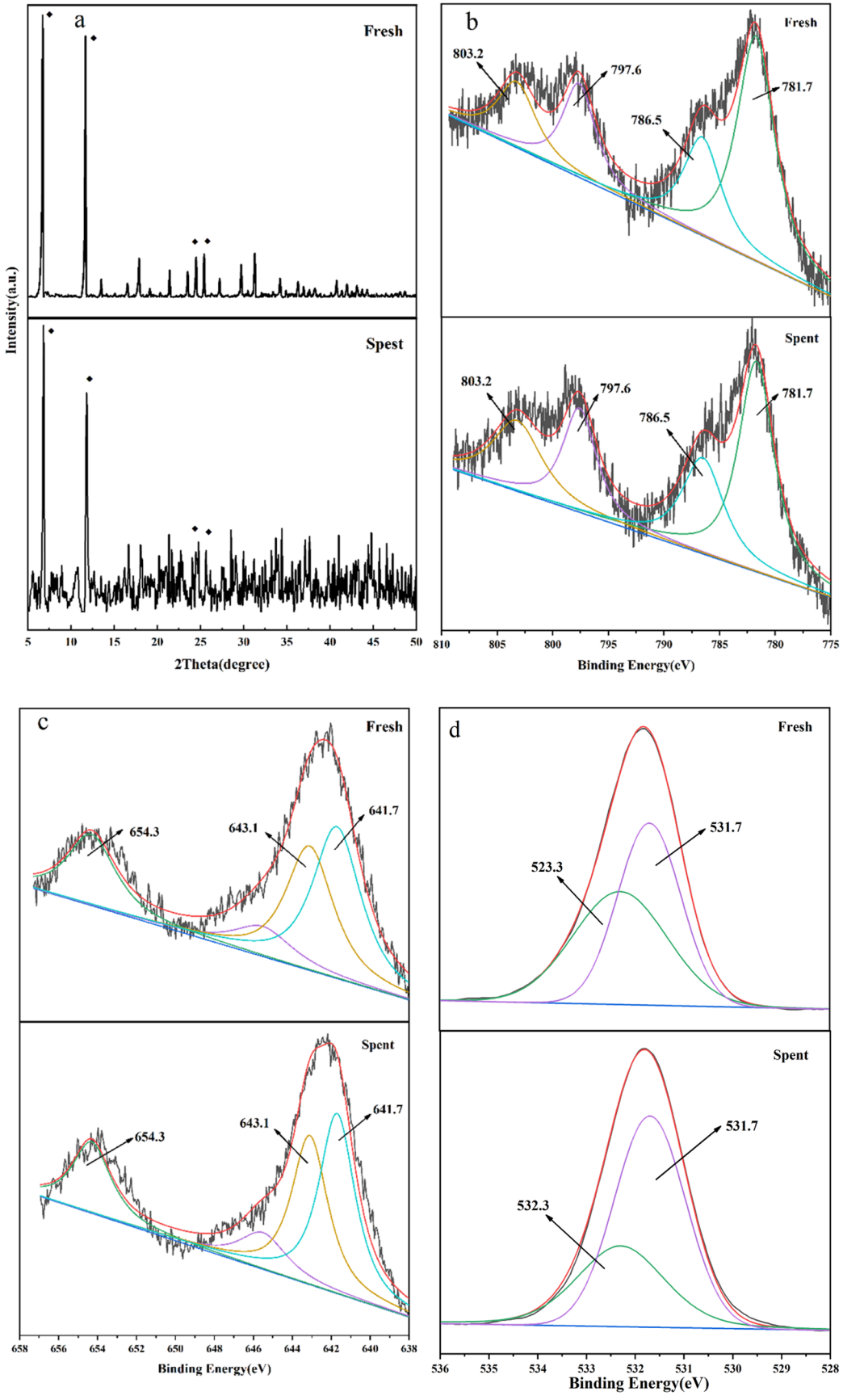

Figure 12. Fresh and spent catalysts: (a) XRD patterns and (b–d) Co XPS (b), Mn XPS (c), and O XPS (d) spectra.

https://doi.org/10.1021/acsomega.1c04077
ACS Omega 2021, 6, 34347−34358

3.7. Conversion Mechanism. Figure 12 compares the XRD and XPS characterizations of the fresh and spent (reacting at 200 °C for 10 h) catalysts. It can be found from Figure 12a that although some impurity peaks appeared on the catalyst after the reaction, the characteristic peaks of the catalyst at 2θ = 6.7, 11.7, 24.4, and 25.7° did not change significantly, indicating that the structure of the catalyst was not destroyed. Figure 12b–d indicates that the element types and valence states on the catalyst surface before and after the reaction did not change, but the results in Table 3 showed that the ratio of Mn^{4+}/Mn^{3+} and Co^{3+}/Co^{2+} in the catalyst decreased after the reaction, indicating that Mn^{4+} and Co^{3+} in NH_3-SCR play a leading role.

Table 3. Relative Atomic Percentages of Different Valence Elements

	percent of valence state % (binding energy, eV)					
catalysts	Mn^{4+}	Mn^{3+}	Co^{3+}	Co^{2+}	Mn^{4+}/Mn^{3+}	Co^{3+}/Co^{2+}
fresh	60.38	39.62	66.99	33.01	1.52	2.03
spent	55.54	44.46	65.41	34.59	1.25	1.89

Figure 13 shows the NH_3-TPD curves of Mn/Co-MOF-74 (Mn/Co = 1:1) at 100–350 °C. There is a clear NH_3 desorption peak on the surface of the Mn/Co-MOF-74 catalyst. The peaks can be divided into three peaks at 171.4 °C (831.1 μmol/g), 236.7 °C (381.0 μmol/g), and 296.9 °C (763.4 μmol/g) (Table 4), indicating that there are three types of acidic centers in Mn/Co-MOF-74 and that Mn/Co-MOF-74 has a strong NH_3 adsorption capacity.

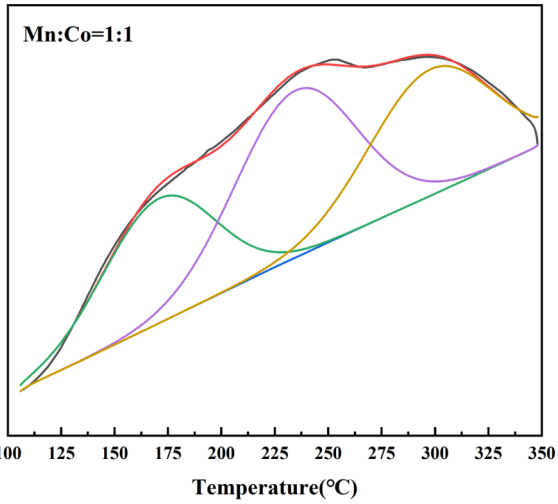

Figure 13. NH_3-TPD curves of Mn/Co-MOF-74 (Mn/Co = 1:1).

Based on the characterization results and related literature, the mechanism of selective catalytic reduction of NO at a low–medium temperature over the Mn/Co-MOF-74 catalyst is speculated as follows: (1) first, gaseous $NH_3(g)$ in the flue gas is adsorbed and converted to adsorbed $NH_3(a)$ by the active sites on the catalyst surface, as depicted in eq 1, which is the prerequisite and key to the catalytic reaction; (2) then, the adsorbed $NH_3(a)$ reacts with the active sites on the catalyst surface containing Co^{3+} and Mn^{4+} to form the intermediates $NH_2(a)$ and H radicals, by which the reduced Co^{2+} and Mn^{3+} ions are generated, as depicted in eqs 2 and 3. It is worth noting that, according to the relevant reports on the Eley–Rideal (E–R) mechanism, $NH_2(a)$ is an important intermediate in the selective catalytic reduction of NO.

(3) Finally, as depicted in eqs 4 and 7, the removal products N_2 and H_2O are produced via the reaction between the intermediate $NH_2(a)$ and gaseous NO; meanwhile, the reduced Co^{2+} and Mn^{3+} ions would also be oxidized to Co^{3+} and Mn^{4+} by oxygen in the flue gas (eqs 5 and 6), thereby ensuring the continuation of the selective catalytic reduction of NO.

Table 4. Amount of Desorption of NH_3 in TPD of Catalysts

peak number	temperature (°C)	quantity (μmol/g)
1	171.4	813.1
2	236.7	381.0
3	296.9	763.4

$$NH_3(g) \rightarrow NH_3(a) \quad (1)$$

$$NH_3(a) + Mn^{4+} \rightarrow NH_2(a) + Mn^{3+} + H \quad (2)$$

$$NH_3(a) + Co^{3+} \rightarrow NH_2(a) + Co^{2+} + H \quad (3)$$

$$NH_2(a) + NO(g) \rightarrow N_2 + H_2O \quad (4)$$

$$Co^{2+} + O_2 \rightarrow Co^{3+} + O \quad (5)$$

$$Mn^{3+} + O_2 \rightarrow Mn^{4+} + O \quad (6)$$

$$H + O \rightarrow H_2O \quad (7)$$

4. CONCLUSIONS

A series of bimetallic Mn/Co-MOF-74 catalysts were successfully synthesized via the microwave hydrothermal method, and the experimental results showed that Mn/Co-MOF-74 with a molar ratio of Mn/Co = 1:1 exhibited the optimal catalytic performance; a 93.5% NO removal efficiency was obtained at 200–225 °C, with a catalyst dosage of 0.2 g, a synthesis temperature of 130 °C, and a synthesis time of 4 h. The abovementioned excellent characteristics could be attributed to the smooth mesoporous structure and the atomic ratios of Mn^{4+}/Mn^{3+} and Co^{3+}/Co^{2+} on the catalyst surface, which played important roles in improving the NO removal efficiency at a low temperature. Furthermore, the Mn/Co-MOF-74 catalyst also exhibited excellent sulfur and water resistances, confirming the feasibility of using bimetal MOF as a new catalyst for the SCR reaction.

AUTHOR INFORMATION

Corresponding Author

Yi Zhao – *School of Environmental Science and Engineering, North China Electric Power University, Beijing 102206, People's Republic of China*; orcid.org/0000-0001-9974-0348; Email: zhaoyi9515@163.com

Authors

Zhonghao Sun – *School of Environmental Science and Engineering, North China Electric Power University, Beijing 102206, People's Republic of China*

Xue Mi – *School of Environmental Science and Engineering, North China Electric Power University, Beijing 102206, People's Republic of China*

https://doi.org/10.1021/acsomega.1c04077
ACS Omega 2021, 6, 34347–34358

Yichen Luo − *School of Environmental Science and Engineering, North China Electric Power University, Beijing 102206, People's Republic of China*
Siyuan Wang − *School of Environmental Science and Engineering, North China Electric Power University, Beijing 102206, People's Republic of China*
Bo Yuan − *School of Environmental Science and Engineering, North China Electric Power University, Beijing 102206, People's Republic of China*
Runlong Hao − *School of Environmental Science and Engineering, North China Electric Power University, Beijing 102206, People's Republic of China*

Complete contact information is available at: https://pubs.acs.org/10.1021/acsomega.1c04077

Notes

The authors declare no competing financial interest.

■ ACKNOWLEDGMENTS

The authors appreciate the financial support by grants from the Key Project of the National Major Research and Development Program of China (2016YFC0203701) and the Fundamental Research Funds for the Central Universities (2019QN091).

■ REFERENCES

(1) Ding, J.; Zhong, Q.; Zhang, S.; Song, F.; Bu, Y. Simultaneous removal of NO_X and SO_2 from coal-fired flue gas by catalytic oxidation-removal process with H_2O_2. *Chem. Eng. J.* **2014**, *243*, 176−182.
(2) Roy, S.; Hegde, M. S.; Madras, G. Catalysis for NO_X abatement. *Appl. Energy* **2009**, *86*, 2283−2297.
(3) Wang, H.; Yuan, B.; Hao, R.; Zhao, Y.; Wang, X. A critical review on the method of simultaneous removal of multi-air-pollutant in flue gas. *Chem. Eng. J.* **2019**, *378*, 122155.
(4) Zhao, Y.; Hao, R.; Yuan, B.; Jiang, J. Simultaneous removal of SO_2, NO and Hg^0 through an integrative process utilizing a cost-effective complex oxidant. *J. Hazard. Mater.* **2016**, *301*, 74−83.
(5) Liu, J.; Wang, L.; Okejiri, F.; Luo, J.; Zhao, J.; Zhang, P.; Liu, M.; Yang, S.; Zhang, Z.; Song, W.; et al. Deep Understanding of Strong Metal Interface Confinement: A Journey of Pd/FeOx Catalysts. *ACS Catal.* **2020**, *10*, 8950−8959.
(6) Zhao, Y.; Yuan, B.; Hao, R.; Tao, Z. Low-Temperature Conversion of NO in Flue Gas by Vaporized H_2O_2 and Nanoscale Zerovalent Iron. *Energy Fuels* **2017**, *31*, 7282−7289.
(7) Yuan, B.; Mao, X.; Wang, Z.; Hao, R.; Zhao, Y. Radical-induced oxidation removal of multi-air-pollutant: A critical review. *J. Hazard. Mater.* **2020**, *383*, 121162.
(8) Gao, F.; Tang, X.; Yi, H.; Zhao, S.; Li, C.; Li, J.; Shi, Y.; Meng, X. A Review on Selective Catalytic Reduction of NO_X by NH_3 over Mn-Based Catalysts at Low Temperatures: Catalysts, Mechanisms, Kinetics and DFT Calculation. *Catal.* **2017**, *7*, 199.
(9) Beale, A. M.; Gao, F.; Lezcano-Gonzalez, I.; Peden, C. H. F.; Szanyi, J. Recent advances in automotive catalysis for NOx emission control by small-pore microporous materials. *Chem. Soc. Rev.* **2015**, *44*, 7371−7405.
(10) Ma, Z.; Yang, H.; Liu, F.; Zhang, X. Interaction between SO_2 and Fe-Cu-Ox/CNTs-TiO_2 catalyst and its influence on NO reduction with NH_3. *Appl. Catal. Gen.* **2013**, *467*, 450−455.
(11) Shen, B.; Liu, T.; Zhao, N.; Yang, X.; Deng, L. Iron-doped Mn-Ce/TiO_2 catalyst for low temperature selective catalytic reduction of NO with NH_3. *J. Environ. Sci.* **2010**, *22*, 1447−1454.
(12) Li, J.; Chang, H.; Ma, L.; Hao, J.; Yang, R. T. Low-temperature selective catalytic reduction of NO_X with NH_3 over metal oxide and zeolite catalysts—A review. *Catal. Today* **2011**, *175*, 147−156.
(13) Jiang, B.; Deng, B.; Zhang, Z.; Wu, Z.; Tang, X.; Yao, S.; Lu, H. Effect of Zr Addition on the Low-Temperature SCR Activity and SO_2 Tolerance of Fe−Mn/Ti Catalysts. *J. Phys. Chem. C* **2014**, *118*, 14866−14875.
(14) Liu, J.; Cheng, H.; Tan, J.; Liu, B.; Zhang, Z.; Xu, H.; Zhao, M.; Zhu, W.; Liu, J.; Zhao, Z. Solvent-free rapid synthesis of porous CeWOx by mechanochemical self-assembly strategy for the abatement of NO_x. *J. Mater. Chem. A* **2020**, *8*, 6717−6731.
(15) Furukawa, H.; Cordova, K. E.; O'Keeffe, M.; Yaghi, O. M. The Chemistry and Applications of Metal-Organic Frameworks. *Sci.* **2013**, *341*, 974.
(16) Lu, W.; Wei, Z.; Gu, Z.-Y.; Liu, T.-F.; Park, J.; Park, J.; Tian, J.; Zhang, M.; Zhang, Q.; Gentle, T., III; et al. Tuning the structure and function of metal−organic frameworks via linker design. *Chem. Soc. Rev.* **2014**, *43*, 5561−5593.
(17) Seoane, B.; Castellanos, S.; Dikhtiarenko, A.; Kapteijn, F.; Gascon, J. Multi-scale crystal engineering of metal organic frameworks. *Coord. Chem. Rev.* **2016**, *307*, 147−187.
(18) Nandasiri, M. I.; Jambovane, S. R.; Mcgrail, B. P.; Schaef, H. T.; Nune, S. K. Adsorption, separation, and catalytic properties of densified metal-organic frameworks. *Coord. Chem. Rev.* **2016**, *311*, 38−52.
(19) Cui, Y.; Li, B.; He, H.; Zhou, W.; Chen, B.; Qian, G. Metal-organic frameworks as platforms for functional materials. *Acc. Chem. Res.* **2016**, *49*, 483−493.
(20) Sun, W.; Lin, L.-C.; Peng, X.; Smit, B. Computational Screening of Porous Metal-Organic Frameworks and Zeolites for the Removal of SO_2 and NO_x from Flue Gases. *Aiche J.* **2014**, *60*, 2314.
(21) Wang, P.; Sun, H.; Quan, X.; Chen, S. Enhanced catalytic activity over MIL-100(Fe) loaded ceria catalysts for the selective catalytic reduction of NOx with NH_3 at low temperature. *J. Hazard. Mater.* **2016**, *301*, 512−521.
(22) Sun, X.; Shi, Y.; Zhang, W.; Li, C.; Zhao, Q.; Gao, J.; Li, X. A new type Ni-MOF catalyst with high stability for selective catalytic reduction of NOx with NH_3. *Catal. Commun.* **2018**, *114*, 104−108.
(23) Kapteijn, F.; Vanlangeveld, A. D.; Moulijn, J. A.; Andreini, A.; Vuurman, M. A.; Turek, A. M.; Jehng, J. M.; Wachs, I. E. Alumina-supported manganese oxide catalysts: I. Characterization: Effect of precursor and loading. *J. Catal.* **1994**, *150*, 94−104.
(24) Tian, W.; Yang, H.; Fan, X.; Zhang, X. Catalytic reduction of NOx with NH_3 over different-shaped MnO_2 at low temperature. *J. Hazard. Materials* **2011**, *188*, 105−109.
(25) Peña, D. A.; Uphade, B. S.; Smirniotis, P. G. TiO_2-supported metal oxide catalysts for low-temperature selective catalytic reduction of NO with NH_3: Evaluation and characterization of first row transition metals. *J. catal.* **2004**, *221*, 421−431.
(26) Fang, J.; Wu, Y.; Lei, B.; Wang, L.; Kao, H. Preparation and catalytic performance of supported Mn-Co/TiO_2 catalyst used for selective reduction of NO with NH_3 at low temperatures. *Acta Sci. Circumstantiae* **2014**, *34*, 849−856.
(27) Boningari, T.; Smirniotis, P. G. Co-doping a metal (Cr, Fe, Co, Ni, Cu, Zn, Ce and Zr) on Mn/TiO_2 catalyst and its effect on the selective reduction of NO with NH_3 at low-temperatures. *Appl. Catal. B* **2011**, *110*, 195−206.
(28) Shi, Y.; Tang, X.; Yi, H.; Gao, F.; Zhao, S.; Wang, J.; Yang, K.; Zhang, R. Controlled Synthesis of Spinel-Type Mesoporous Mn−Co Rods for SCR of NOx with NH_3 at Low Temperature. *Ind. Eng. Chem. Res.* **2019**, *58*, 3606−3617.
(29) Jiang, H.; Niu, Y.; Wang, Q.; Chen, Y.; Zhang, M. Single-phase SO_2-resistant to poisoning Co/Mn-MOF-74 catalysts for NH_3-SCR. *Catal. Commun.* **2018**, *113*, 46−50.
(30) Jiang, H.; Wang, C.; Wang, H.; Zhang, M. Synthesis of highly efficient MnOx catalyst for low-temperature NH_3-SCR prepared from Mn-MOF-74 template. *Mater. Lett.* **2016**, *168*, 17−19.
(31) Xie, S.; Qin, Q.; Liu, H.; Jin, L.; Wei, X.; Liu, J.; Liu, X.; Yao, Y.; Dong, L.; Li, B. MOF-74-M (M = Mn, Co, Ni, Zn, MnCo, MnNi, and MnZn) for Low-Temperature NH_3-SCR and In Situ DRIFTS Study Reaction Mechanism. *ACS Appl. Mater. Interfaces* **2020**, *12*, 48476−48485.

(32) Botas, J. A.; Calleja, G.; Sánchez-Sánchez, M.; Gisela Orcajo, M. Effect of Zn/Co ratio in MOF-74 type materials containing exposed metal sites on their hydrogen adsorption behaviour and on their band gap energy. *Int. J. Hydrogen Energy* **2011**, *36*, 10834−10844.
(33) Lian, Q.; Roy, A.; Kizilkaya, O.; Gang, D. D.; Holmes, W.; Zappi, M. E.; Zhang, X.; Yao, H. Uniform Mesoporous Amorphous Cobalt-Inherent Silicon Oxide as a Highly Active Heterogeneous Catalyst in the Activation of Peroxymonosulfate for Rapid Oxidation of 2,4-Dichlorophenol: The Important Role of Inherent Cobalt in the Catalytic Mechanism. *ACS Appl. Mater. Interfaces* **2020**, *12*, 57190−57206.
(34) Sun, K.; Liu, Z.; Song, S.; Liu, W.; Wang, P.; Zhang, T.; Xue, Y.; Wang, Y.; Tan, Y. Effect of Hydroxyl Groups on CuCoMg Nanosheets for Ethanol and Higher Alcohol Synthesis from Syngas. *Ind. Eng. Chem. Res.* **2021**, *60*, 2388−2399.
(35) Bui, N.-Q.; Geantet, C.; Berhault, G. Maleic acid, an efficient additive for the activation of regenerated $CoMo/Al_2O_3$ hydrotreating catalysts. *J. Catal.* **2015**, *330*, 374−386.
(36) Shen, Q.; Zhang, L.; Sun, N.; Wang, H.; Zhong, L.; He, C.; Wei, W.; Sun, Y. Hollow MnOx-CeO_2 mixed oxides as highly efficient catalysts in NO oxidation. *Chem. Eng. J.* **2017**, *322*, 46−55.
(37) Sun, H.; Yu, X.; Ma, X.; Yang, X.; Lin, M.; Ge, M. MnO_x-CeO_2 catalyst derived from metal-organic frameworks for toluene oxidation. *Catal. Today* **2020**, *355*, 580−586.
(38) Kryuchkova, N. A.; Kostin, G. A.; Korotaev, E. V.; Kalinkin, A. V. XPS and quantum chemical investigation of electronic structure of Co complexes with calix [4] arenes modified by R_2PO groups in upper or lower rim. *J. Electron Spectrosc. Relat. Phenom.* **2018**, *229*, 114−123.
(39) Alburquenque, D.; Troncoso, L.; Denardin, J. C.; Marco, J. F.; Gautier, J. L. Cation distribution and magnetic properties of $Ni_xMn_{3-x}O_4$-delta (X=0.5, 0.75) synthesized by an ultrasound method. *J. Phys. Chem. Soilds* **2019**, *134*, 89−96.
(40) Wu, Z.; Jin, R.; Liu, Y.; Wang, H. Ceria modified MnOx/TiO_2 as a superior catalyst for NO reduction with NH_3 at low-temperature. *Catal. Commun.* **2008**, *9*, 2217−2220.
(41) Biesinger, M. C.; Payne, B. P.; Grosvenor, A. P.; Lau, L. W. M.; Gerson, A. R.; Smart, R. S. C. Resolving surface chemical states in XPS analysis of first row transition metals, oxides and hydroxides: Cr, Mn, Fe, Co and Ni. *Appl. Surf. Sci.* **2011**, *257*, 2717−2730.
(42) Zhang, L.; Shi, L.; Huang, L.; Zhang, J.; Gao, R.; Zhang, D. Rational Design of High-Performance DeNOx Catalysts Based on $Mn_xCo_{3-x}O_4$ Nanocages Derived from Metal−Organic Frameworks. *ACS catal.* **2014**, *4*, 1753−1763.
(43) Chuang, C.-M.; Huang, C.-W.; Teng, H.; Ting, J.-M. Effects of Carbon Nanotube Grafting on the Performance of Electric Double Layer Capacitors. *Energy Fuel* **2010**, *24*, 6476−6482.
(44) Li, X.; He, C.; Zheng, J.; Wu, D.; Duan, Y.; Li, Y.; Rao, P.; Tang, B.; Rui, Y. Flocculent Cu Caused by the Jahn−Teller Effect Improved the Performance of Mg-MOF-74 as an Anode Material for Lithium-Ion Batteries. *ACS Appl. Mater. Interfaces* **2020**, *12*, 52864−52872.
(45) Jiang, H.; Wang, Q.; Wang, H.; Chen, Y.; Zhang, M. MOF-74 as an Efficient Catalyst for the Low-Temperature Selective Catalytic Reduction of NOx with NH_3. *ACS Appl. Mater. Interfaces* **2016**, *8*, 26817−26826.

https://doi.org/10.1021/acsomega.1c04077
ACS Omega 2021, 6, 34347−34358